Supporting Information

Neutron diffraction reveals hydrogen bonds critical for cGMP-selective activation: Insights for protein kinase G agonist design

Gilbert Y. Huang, Oksana O. Gerlits, Matthew P. Blakeley, Banumathi Sankaran, Andrey Y. Kovalevsky and Choel Kim

Supplementary Experimental Methods Section

Materials and Methods

Expression, Crystallization, and data collection. PKG Iβ 219-369 (CNB-B) was expressed and purified as previously described(*1*). For the XN structure, the CNB-B crystals were grown in 200 μL drops made by mixing the complex (with ~35 mg/mL of PKG Iβ), the reservoir (1.6 M Na_3Citrate, pH 6.5 in H_2O) and 1 M NaI solutions at a 1:0.8:0.2 ratio in the 9-well glass plate/sandwich box sitting drop setup. A crystal suitable for neutron diffraction measured 0.7 × 0.8 × 1.7 mm (~0.95 mm^3) and was mounted in a quartz capillary containing the reservoir solution made with 100% D_2O. Another crystal from the same crystallization drop that provided the crystal for neutron data collection was mounted in the same fashion for room-temperature X-ray data collection. The labile hydrogen atoms were allowed to exchange with deuterium by vapor diffusion for several

weeks for both crystals before starting data collection. Quasi-Laue neutron data to 2.2 Å resolution were collected from the 0.95 mm^3 PKG Iβ-cGMP crystal at room temperature on the LADI-III beamline at the Institut Laue-Langevin(*2*) (Figure S6). As is usual for a Laue experiment, the crystal was held stationary at a different φ setting for each exposure. In total 17 images were collected (with an average exposure time of 24 h per image) from 3 different crystal orientations. The neutron data were processed using the Daresbury Laboratory *LAUE* suite program *LAUEGEN(3)* modified to account for the cylindrical geometry of the detector(*4*). The program *LSCALE(5)* was used to determine the wavelength-normalization curve using the intensities of symmetry-equivalent reflections measured at different wavelengths. No explicit absorption corrections were applied. These data were then merged in *SCALA(6)*. Monochromatic X-ray diffraction data were collected using a Rigaku HomeFlux system, equipped with a MicroMax-007 HF generator and Osmic VariMax optics. The diffraction images were obtained using an RAXIS-IV++ image-plate detector. Diffraction data were collected, integrated and scaled using HKL3000 software suite(*7*). The room-temperature X-ray structure of PKG Iβ-cGMP was refined using *SHELX-97(8)* at the resolution of 1.76 Å before using it as a starting model in joint XN refinement. A summary of the experimental and refinement statistics is given in Supporting Table 1.

For the low-temperature PKGIβ-cAMP crystals, purified PKG Iβ was concentrated to 125mg/mL, and cAMP was dissolved in the sample to a final concentration of 20mM. Crystals were grown in 5μL drops by mixing 2.5μL protein/cAMP solution with 2μL of 1.6 M Na_3Citrate, pH 6.5 and 0.5μL 1M NaI, and this drop was sealed over a reservoir containing 1.6 M Na_3Citrate, pH 6.5. Crystal growth was observed after 2 months, and

crystals were cryo-protected with paratone-N before being flash-frozen. Diffraction data were collected at the Advanced Light Source (Berkeley, CA). Diffraction data was integrated and scaled using HKL2000, and the structure was solved using PDB:4KU7 as a search model and refined using phenix.refine(*9*) with cycles of model building performed manually in Coot(*10*). The coordinates of CNB-B:cAMP have been deposited into the PDB (ID: 4QX5).

Joint XN structure refinement. The joint XN structure of PKG Iβ-cGMP was determined using *nCNS(11)* and manipulated in *Coot(10)*. After initial rigid-body refinement, several macrocycles of positional, atomic displacement parameter, and occupancy refinement followed. Between each macrocycle the structure was checked, side-chain conformations were altered and water molecule orientations were built based on the F_O-F_C difference neutron scattering density map. The $2F_O$-F_C and F_O-F_C neutron scattering density maps were then examined to determine the correct orientation of hydroxyl (Ser, Thr, Tyr) and ammonium (Lys) groups, and protonation states of His and Lys residues. The protonation states of some disordered side chains could not be obtained directly, and remained ambiguous. All water molecules were refined as D_2O. Initially, water oxygen atoms were positioned according to their electron density peaks, and then were shifted slightly in accordance with the neutron scattering density maps. The level of H/D exchange at OH, NH and SH sites were refined. All labile H positions in PKG Iβ and cGMP were modelled as D and then the occupancy of D was allowed to refine within the range of -0.56 to 1.00 (the scattering length of H is -0.56 times the scattering length of D). Before depositing the final structure to the PDB, a script was run that converts a record for the coordinate of D atom into two records corresponding to an H and a D atom

partially occupying the same site, both with positive partial occupancies that add up to unity. The Ramachandran statistics for the PKG Iβ-cGMP structure reported here are as follows: residues in most favored regions 97.6%, residues in additional allowed regions 2.4%. Ser290 and Glu291 were not visible in either electron or nuclear density maps, and therefore were not modelled in the joint XN refinement. The joint XN structure of PKG Iβ-cGMP has been deposited to the Protein Data Bank (PDB: 4QXK).

Supplementary Figures and Tables

Figure S1.

Larger version of Figure 1. PKG Iβ (219-369):cGMP and PKG Iβ (219-369):cAMP complexes. (A) XN structure of PKG Iβ (219-369):cGMP at room temperature (293 K), with interacting side chains rendered in sticks and colored by atom type, with carbon gray, oxygen red, nitrogen blue, hydrogen black, and deuterium magenta. The 2|Fo|-|Fc| nuclear density for cGMP (*syn*) is contoured at 1σ and shown as a gray mesh. (B) X-ray structure PKG Iβ (219-369):cAMP at low temperature (100 K). The 2|Fo|-|Fc| electron density map for cAMP (*anti* and *syn*) is contoured at 1σ and shown as a gray mesh.

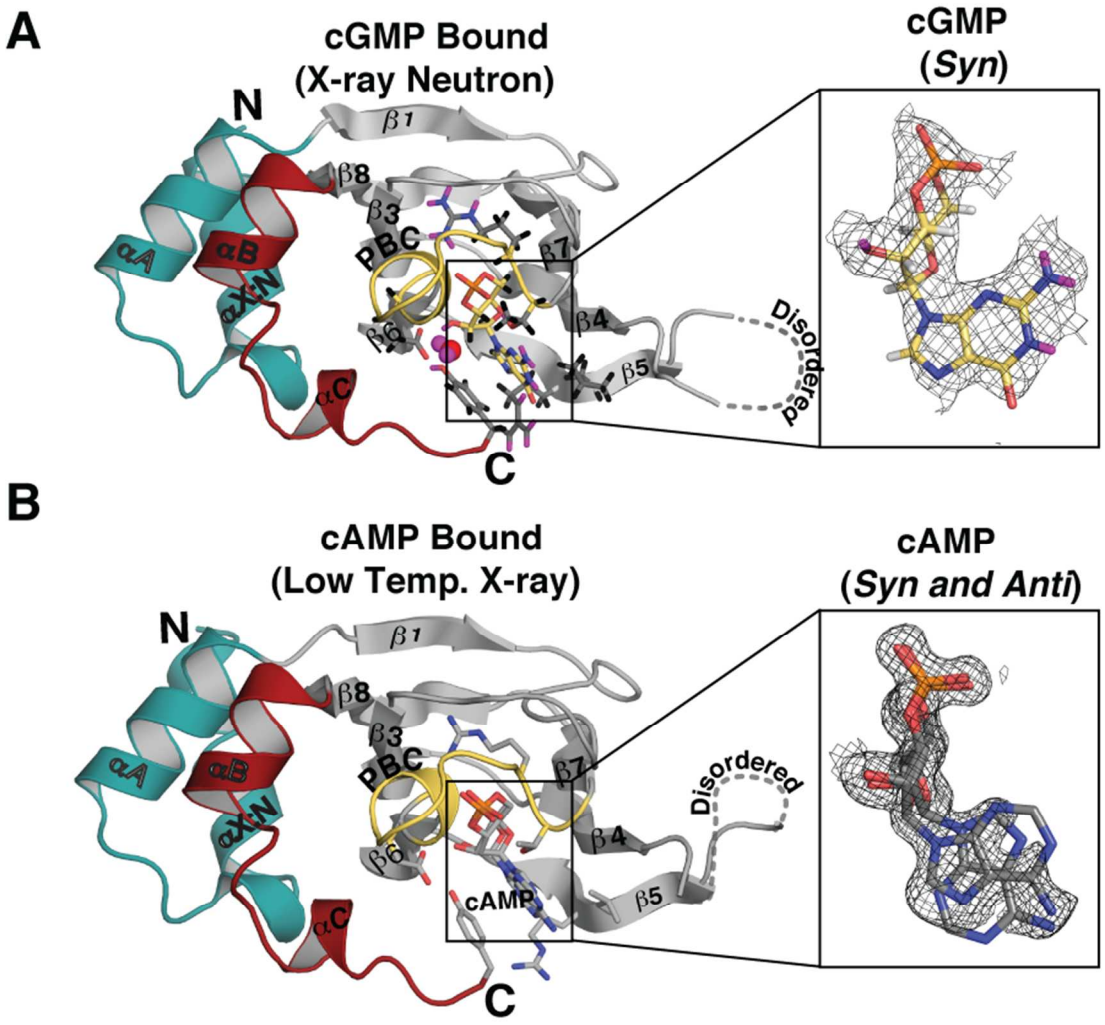

Figure S2. Detailed interactions between the CNB-B domain and cyclic nucleotides. (A) Interactions between cGMP complete with positions of hydrogen (black sticks) and deuterium (magenta) resolved by neutron crystallography. Only strands β 4/5, the PBC and the αB/αC helices are shown. Hydrogen bonds are marked with dashed lines and their distances are shown in Ångstroms. Zoomed-in views of the interactions with cGMP are shown on either side. The side chains and D_2O are rendered as sticks and spheres, respectively, and colored as previously described in Figure 1. (B) Interactions between CNB-B and cAMP seen at 100K. Zoomed-in views of the interactions with cAMP are shown on either side. The adenine moiety of cAMP and side chains of Arg297 and Tyr351 are shown with transparent surface with their distances marked with dashed arrows. A water molecule in the binding pocket is shown as a red sphere.

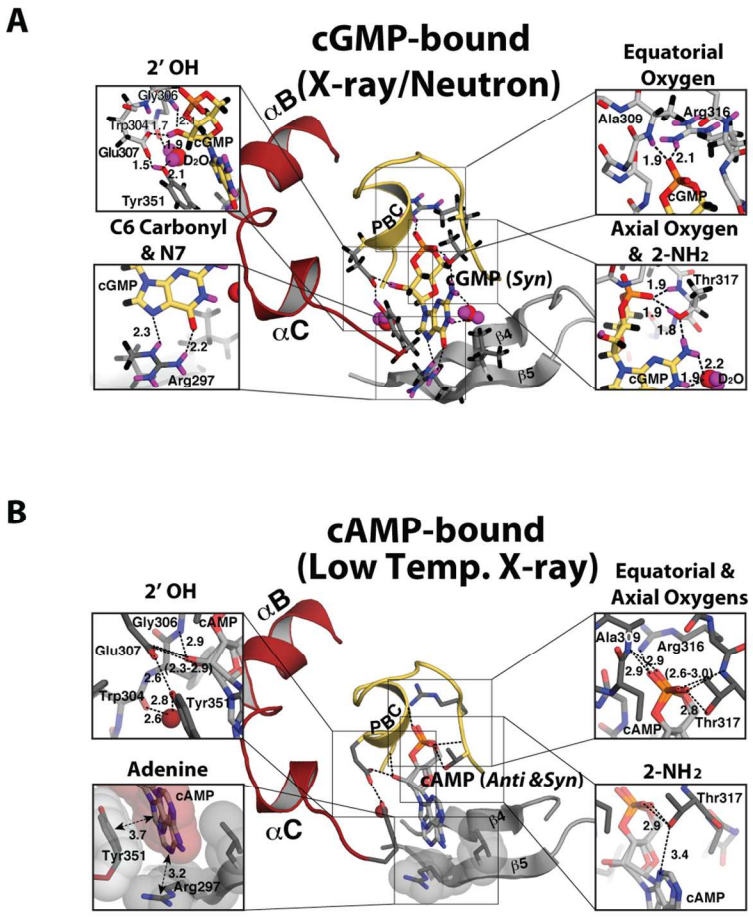

Figure S3.

Larger version of Figure 2. XN versus low temperature X-ray structures. (A) Room temperature XN (left, PDB:4QXK) and low-temperature X-ray structures (PDB:4KU7) bound to cGMP (right). (B) Superposition of the XN (black) and low temperature structures (red-cGMP bound, cyan-cAMP bound) in stereo. (C) cGMP pocket and interacting residues in stereo.

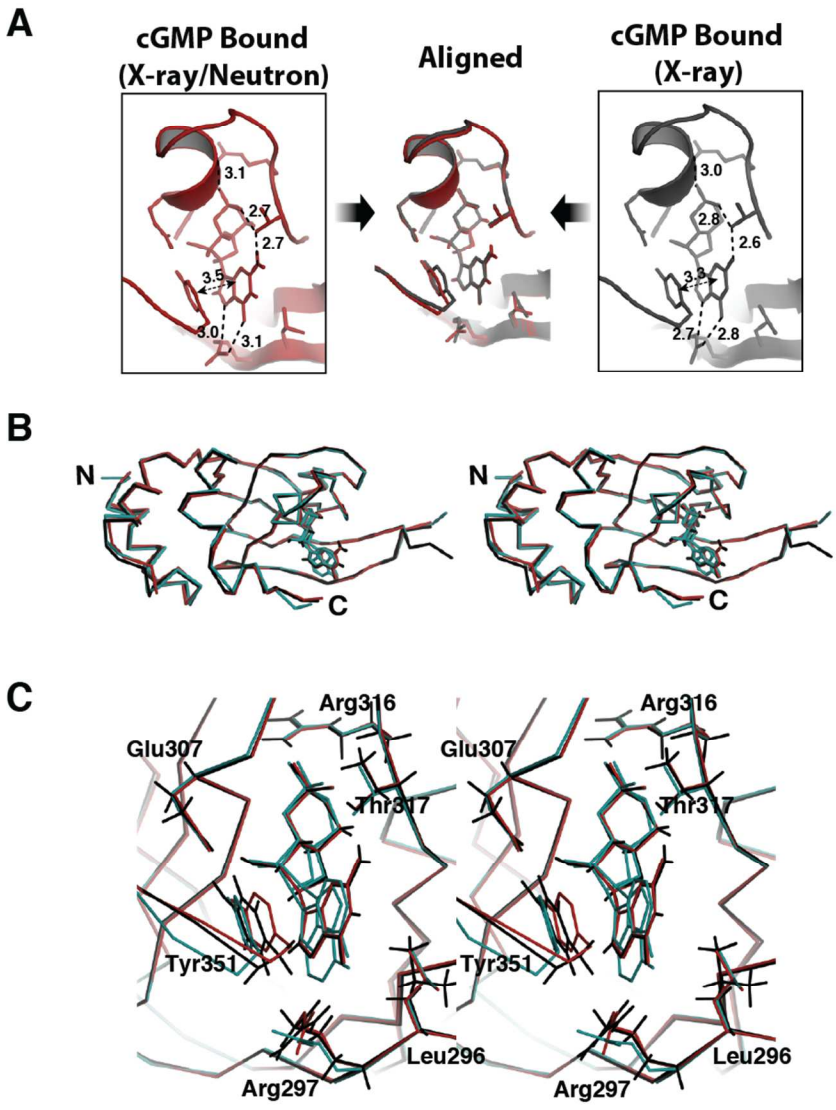

Figure S4.

Omit map contoured at 3.5σ showing density (blue mesh) for deuteriums on Thr317, Tyr351, and the 2'-OD of cGMP.

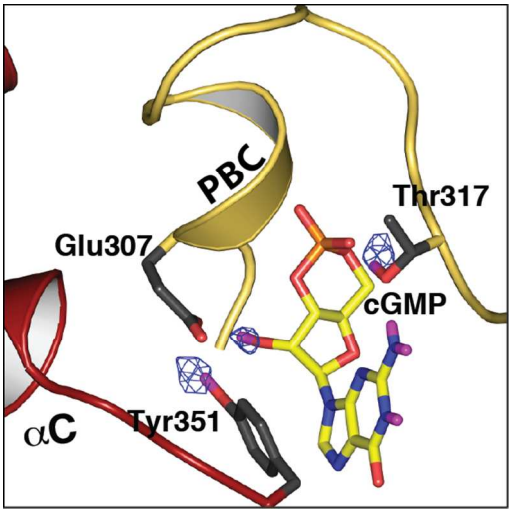

Figure S5. Conformational change associated with cGMP binding at the PBC region. Crystal structures of the CNB-B domain in apo (PDB code : 4KU8) and cGMP bound (PDB code :4KU7) conformations are superimposed at the β barrel and only the PBC regions are shown. The apo conformation is colored in gray and the cGMP bound in yellow. The backbone amide of Ala309 is marked with blue circle.

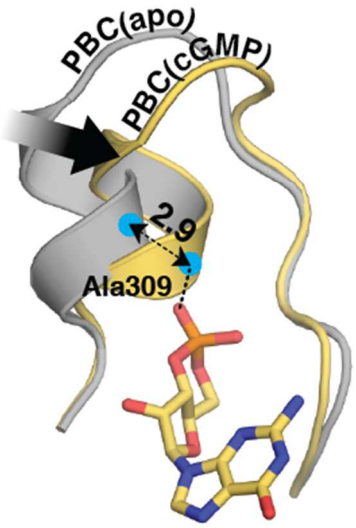

Figure S6. Quasi-Laue neutron diffraction image obtained from the PKG Iβ-cGMP crystal used for data collection after a 24 hour exposure.

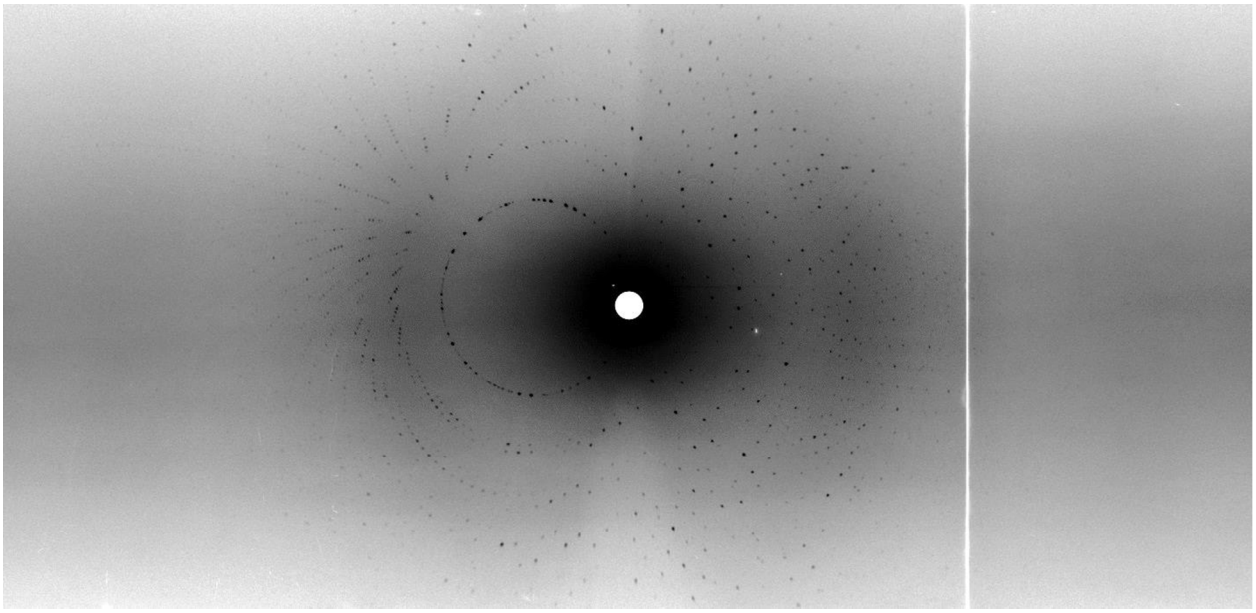

Figure S7. Conformational changes that occur upon cAMP binding. (A) PBC, β4, β5, αB, and αC regions are shown for apo CNB-B (PDB: 4KU8, chain A) and cAMP-bound CNB-B (PDB: 4QX5). Large rearrangement of the αB and αC helices occur upon cAMP binding, which causes repositioning of Tyr351 to the binding pocket. (B) Structural alignment of apo CNB-B and cAMP-bound CNB-B at the β-barrel. Additional conformational changes in the side chain of Arg297 and the PBC are observed upon cAMP binding.

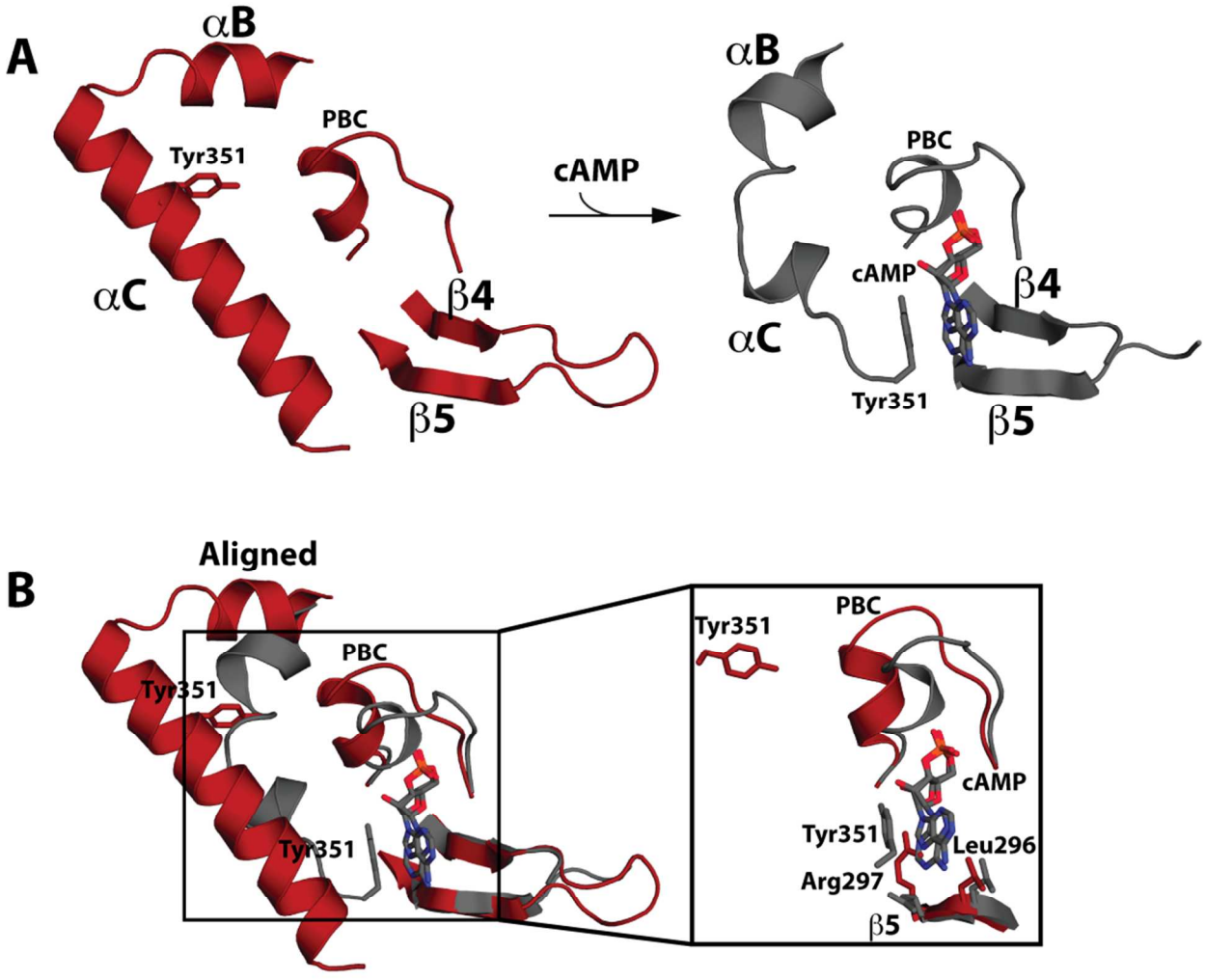

Figure S8. Fo-Fc electron density for cAMP contoured at 3.0σ. Full electron density is observed for the cyclic phosphate and ribose moieties, while partial density is observed for the purine moiety suggesting multiple conformations.

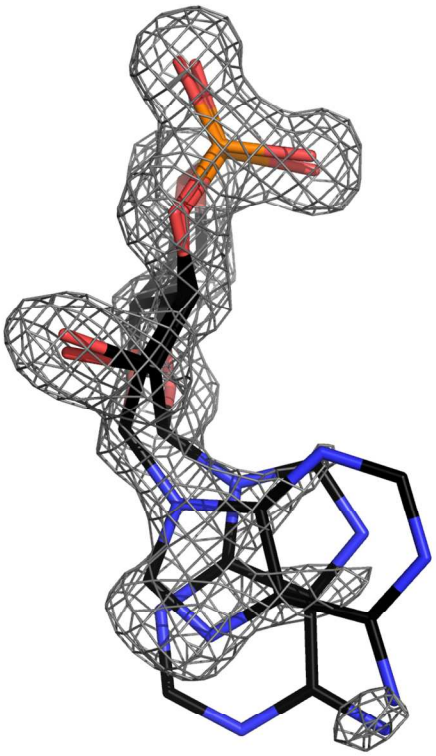

Table S1. Data collection and refinement statistics.

	PKG Iβ-cGMP	PKG Iβ-cGMP	PKG Iβ-cAMP
Data collection	*Room temp. X-ray*	*Room temp. Neutron*	*Low temp. X-ray*
Beamline/Facility	Rigaku HomeFlux	LADI-III/ILL	ALS 5.0.1
Space group	$P4_12_12$	$P4_12_12$	$P4_12_12$
Cell dimensions			
a, *b*, *c* (Å)	48.75, 48.75, 104.86	48.75, 48.75, 104.86	48.44, 48.44, 103.46
α, β, γ (°)	90, 90, 90	90, 90, 90	90, 90, 90
Resolution (Å)	40.00 – 1.76 (1.82-1.76)*	40.00-2.20 (2.32-2.20)*	50-1.32 (1.34-1.32)*
No. reflections measured		25790	894917
No. reflections unique	13053 (1254)	5851	29877
R_{merge}	0.574 (0.044)	0.085 (0.227)	0.055 (0.517)
I / σI	35.0 (2.8)	4.4 (3.2)	31.1(6.0)
Completeness (%)	98.7 (97.8)	85.8 (73.9)	99.4(99.4)
Redundancy	7.3 (6.6)	2.5 (2.0)	13.6(13.7)
Data rejection criteria		no observation & |F|=0	no observation & |F|=0
		Joint XN Refinement	**X-ray Refinement**
Resolution (neutron, Å)		40-2.20	N/A
Resolution (X-ray, Å)		40-1.76	50-1.32
Sigma cut-off		2.5	detector limit
No. reflections (neutron)		5552	n/a
No. reflections (X-ray)		11345	29770
R_{work} / R_{free} (neutron)		0.277 / 0.318	n/a
R_{work} / R_{free} (X-ray)		0.257 / 0.269	0.201 / 0.223
No. atoms			
Protein including H/D		1990	1020
Other		1	20
Ligand		34	22
Water		333 (111 D_2Os)	118
B-factors			
Protein		26.5	24.6
Other		17.1	38.5
Ligand		25.3	21.0
Water		39.1	29.9
R.m.s. deviations			
Bond lengths (Å)		0.008	0.006
Bond angles (°)		1.175	1.189

Table S2. Bond distances between protein and ligand.

Bond distances	CNB-B Residue Atom	XN cGMP-bound		cAMP-bound *syn*		cAMP-bound *anti*	
		cGMP atom	Distance from Atom (Å)	cAMP atom	Distance from atom (Å)	cAMP atom	Distance from atom (Å)
	Arg297 NE	N7	3.0	N7	4.6	N1	3.1
	Arg297 DE	N7	2.3	n/a	n/a	n/a	n/a
	Arg297 NH2	O6	3.1	N6	4.5	N1 N6	4.2 4.0
	Arg297 DH21	O6	2.2	n/a	n/a	n/a	n/a
	Gly306 N	O2'	2.9	O2'	2.9	O2'	2.9
	Gly306 DN	O2'	2.1	n/a	n/a	n/a	n/a
	Glu307 OE1	O2'	2.4	O2'	2.3	O2'	2.9
	Glu307 OE1	DO2'	1.7	n/a	n/a	n/a	n/a
	Ala309 N	O1A	2.9	O2P	3.1	O2P	3.0
	Ala309 DN	O1A	1.9	n/a	n/a	n/a	n/a
	Arg316 NH1	O1A	3.1	O2P	2.9	O2P	2.9
	Arg316 DH11	O1A	2.1	n/a	n/a	n/a	n/a
	Thr317 N	O2A	2.9	O1P	2.6	O1P	3.0
	Thr317 DN	O2A	1.9	n/a	n/a	n/a	n/a
	Thr317 OG1	O2A	2.8	O1P	2.7	O1P	2.9
		N2	2.7	C2	3.3	C8	3.6
		D3	1.8	n/a	n/a	n/a	n/a
	Thr317 DG1	O2A	1.9	n/a	n/a	n/a	n/a

Supplementary Material References

1. Huang, G. Y., Kim, J. J., Reger, A. S., Lorenz, R., Moon, E. W., Zhao, C., Casteel, D. E., Bertinetti, D., Vanschouwen, B., Selvaratnam, R., Pflugrath, J. W., Sankaran, B., Melacini, G., Herberg, F. W., and Kim, C. (2014) Structural basis for cyclic-nucleotide selectivity and cGMP-selective activation of PKG I, *Structure 22*, 116-124.
2. Blakeley, M. P., Teixeira, S. C., Petit-Haertlein, I., Hazemann, I., Mitschler, A., Haertlein, M., Howard, E., and Podjarny, A. D. (2010) Neutron macromolecular crystallography with LADI-III, *Acta Crystallogr D Biol Crystallogr 66*, 1198-1205.
3. Campbell, J. (1995) LAUEGEN, an X-windows-based program for the processing of Laue diffraction data, *Journal of Applied Crystallography 28*, 228-236.
4. Campbell, J., Hao, Q., Harding, M., Nguti, N., and Wilkinson, C. (1998) LAUEGEN version 6.0 and INTLDM, *Journal of Applied Crystallography 31*, 496-502.
5. Arzt, S., Campbell, J., Harding, M., Hao, Q., and Helliwell, J. (1999) LSCALE - the new normalization, scaling and absorption correction program in the Daresbury Laue software suite, *Journal of Applied Crystallography 32*, 554-562.
6. Weiss, M. (2001) Global indicators of X-ray data quality, *Journal of Applied Crystallography 34*, 130-135.
7. Minor, W., Cymborowski, M., Otwinowski, Z., and Churszcz, M. (2006) HKL3000: the integration of data reduction and structure solution - from diffraction images to an initial model in minutes, *Acta Crystallogr D Biol Crystallogr D62*, 859-866.
8. Sheldrick, G. (2008) A short history of SHELX, *Acta Crystallographica Section A 64*, 112-122.
9. Afonine, P., Grosse-Kunstleve, R., Echols, N., Headd, J., Moriarty, N., Mustyakimov, M., Terwilliger, T., Urzhumtsev, A., Zwart, P., and Adams, P. (2012) Towards automated crystallographic structure refinement with phenix.refine, *Acta Crystallogr D Biol Crystallogr 68*, 352-367.
10. Emsley, P., Lohkamp, B., Scott, W., and Cowtan, K. (2010) Features and development of Coot, *Acta Crystallogr D Biol Crystallogr 66*, 486-501.
11. Adams, P., Mustyakimov, M., Afonine, P., and Langan, P. (2009) Generalized X-ray and neutron crystallographic analysis: more accurate and complete structures for biological molecules, *Acta Crystallogr D Biol Crystallogr 65*, 567-573.